Lab on a Chip

View Online
Dynamic Article Links

Cite this: *Lab Chip*, 2011, **11**, 2397

www.rsc.org/loc

PAPER

Pneumatically tunable optofluidic 2 × 2 switch for reconfigurable optical circuit†

Wuzhou Song* and Demetri Psaltis

Received 11th March 2011, Accepted 28th April 2011
DOI: 10.1039/c1lc20220k

We presented a pneumatically tunable 2 × 2 optofluidic switch for on-chip light routing that was controlled by compressed air. The device was fabricated with an optically clear elastomer—polydimethylsiloxane (PDMS)—by soft-lithography. The optical switching is realized with a tunable air-gap mirror by which the light is deflected due to total internal reflection in the bypass state. When the device is subjected to high pressure, the air gap collapses and hence the light will be switched to the crossover state. The device had a switching speed of more than 5 Hz and an extinction ratio of 8 dB. This switch can be readily integrated with other microfluidic circuits. We demonstrated a simple reconfigurable optical waveguide circuit for dual-channel microfluidic spectroscopy measurement on a chip.

1. Introduction

The convergence of microfluidic and optics led to the emergence of optofluidics where a number of optical devices have been realized.[1,2] Optical and microfluidic components have been built on the same chip through optofluidic integration. Optical components such as lenses, mirrors, optical traps, liquid waveguides and light sources have been demonstrated.[3–20] Reconfigurability is another major advantage of optofluidics by which one can change the optical properties of the device by simply manipulating the fluids. Compared with rigid optical systems made of glasses, metals and semiconductors, optofluidic devices exhibit unique tunability due to the nature of fluids which offer a wide choice of compositions and shapes.[21,22] For example, tunable photonics crystal and microfluidic dye lasers have been reported by changing the refractive index of liquids;[23,24] tunable liquid lenses and electronic paper were realized utilizing the electrowetting effect;[25,26] liquid–liquid waveguides were demonstrated based on flowing liquids with different indices of refraction.[27,28] Optical waveguides have been integrated in microfluidic chips for manipulation and detection of bio-chemical samples.[29–31] The optical switch plays a crucial role towards reconfigurable optofluidic circuits in which multiple components are integrated on a single optofluidic chip. Unlike the traditional optical switches designed for communications that are high cost and high speed, the primary requirement for optofluidic switches is simple fabrication that is compatible with integration with other components on the chip. Recently a 2 × 2 optical switch was demonstrated based on tuning of refractive index of liquid in a PDMS microchannel.[32]

This switch relied on complex design for flow control. Several 1 × 2 optofluidic switches had been also demonstrated based on the liquid–core/liquid cladding waveguiding system formed by laminar flow.[9,33,34] These methods rely on accurate flow control and hence increase the control complexity. In addition, continual flow of fluids was required during operation. Thus a simple design of optofluidic switch with easy operation is desirable. We have recently introduced a pneumatically tuning mechanism for the optofluidic dye laser in which the lasing wavelength can be tuned by air pressure.[35] Pneumatic tuning of optofluidic devices has the benefit of easy control since it employs a tuning mechanism that is readily available in the microfluidic platform.[36] In this work, we present a pneumatically tunable 2 × 2 optical switch in which an air-gap mirror was switchable for light routing. The switch was fabricated on a polydimethylsiloxane (PDMS) chip and controlled by air pressure. Based on this switch, we also used to demonstrate a simple reconfigurable optical circuit for dual-channel absorption spectroscopy on a chip.

2. Working principle of optofluidic switch

Fig. 1 shows schematically the top view of the device. The chip was made with a clear elastomer (PDMS). The device contains the input and output waveguides in a four port configuration and an air filled micro-channel in the center which serves as the switchable air-gap mirror. The working principle is similar to the optical switch reported by Agilent Inc. where they used an air-bubble for beam deflection.[37] Fig. 1(a) and (b) correspond to the optical switch in bypass and crossover modes respectively. The microfluidic channel adjacent to the air-gap is filled with liquid

School of Engineering, Swiss Federal Institute of Technology Lausanne (EPFL), CH-1015 Lausanne, Switzerland. E-mail: wuzhou.song@epfl.ch; Fax: +41 21 6936930; Tel: +41 21 6935181

† Electronic supplementary information (ESI) available: S1: demonstration movie of the device. See DOI: 10.1039/c1lc20220k

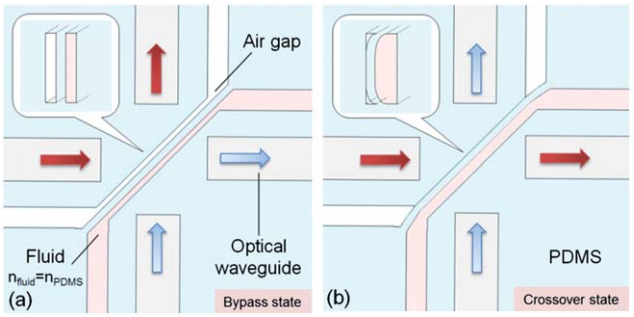

Fig. 1 Top view of the device at the switching mode of crossover (a) and bypass (b); the insets show the cross-sectional view of the air-gap channel.

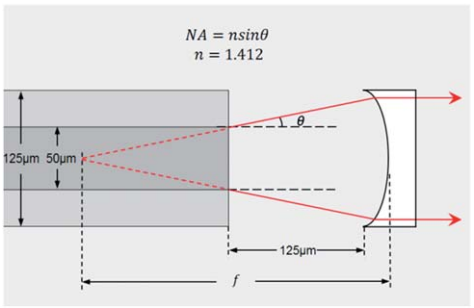

Fig. 3 The schematic of an integrated lens for compensating the divergence of the beam from the fiber end.

that has the same refractive index as PDMS. In between these two channels, the thin PDMS membrane can be deformed when pressure is applied to the liquid. In the crossover mode no pressure is applied to the liquid. The refractive index of PDMS is 1.412 which is much higher than the air; the critical angle for total internal reflection is 45.1°. In this design, as shown in Fig. 2, we carefully chose 45.5° of the incident angle which is slightly larger than the critical angle. Thus, in theory, the two incident beams can be totally deflected at the PDMS–air interfaces of the air-gap mirror. When pressure is applied to liquid, the PDMS membrane is deformed until the air-gap collapses. The schematic of cross-section view of the air-gap mirror and microfluidic channel is shown in the inset of Fig. 1(a) and (b). As the PDMS is a soft material, when the two surfaces of PDMS make contact the air-gap will be vanished and hence the light can go through it without any reflection or refraction. As a result, the light beams get switched from bypass mode to crossover states. When the pressure applied on liquid is released, the PDMS membrane will bounce back due to the elasticity of PDMS. In this experiment, the liquid was pressurized by compressed air; hence in fact the switch was pneumatically controlled.

In addition, as the output beam from the end of the fiber has a small divergence angle, we added an integrated tunable micro-lens to focus the beam and hence compensate the divergence, as shown in Fig. 3. As the multimode fiber has a numerical aperture (NA) of 0.22, the half divergence angle is to be 10°. Based on our calculation, we estimated that the optimal focal length of the micro-lens should be around 300 μm to get parallel output beam.

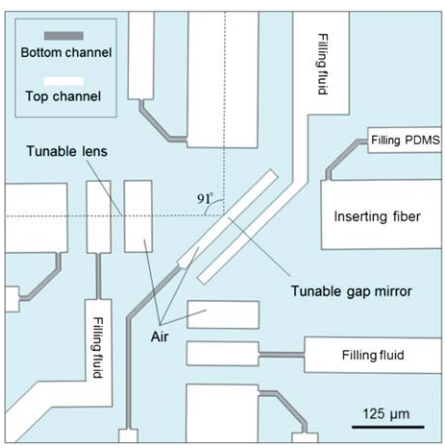

Fig. 2 Top view of the dual layer structure of the optofluidic switch where the gray color represents the channels with 20 μm thickness; the white color represents the channels with 125 μm thickness.

3. Fabrication of optofluidic switch

Two different chips were fabricated in this experiment. The first is a simple 2 × 2 optofluidic switch, and the second is a reconfigurable circuit by integrating the optofluidic switches with other components. Both devices have similar design and the same fabrication process. The chip was assembled with a structured PDMS layer with a flat PDMS layer. The structured PDMS layer was cast from an SU-8 mold patterned on a silicon wafer. The mold had a two layer structure fabricated by UV photolithography. Fig. 2 shows the layout of the chip. The channels filled with gray color were cast from the bottom layer of the mold (thickness 15 μm). The parts filled with white color were cast from the upper layer of the mold and they have a higher thickness (125 μm). Each fiber port has the same width (125 μm) that equals the width of the fiber. The purpose of the bottom layer of the mold was to define the microfluidic channel for liquid delivery; meanwhile, it can reduce the asymmetric deformation during mold fabrication and device operation when the liquids pressurize channels. The upper layer of the mold defines the air-gap mirror and the fiber ports.

The silicon wafer was first spin-coated with a 15 μm thick layer of negative photoresist (SU-8 1060, Gersteltec), then it was exposed to UV-light through a mask and developed. After hard-baking on a hotplate at 120 °C for half hour, the wafer was spin-coated with a second layer of 125 μm thickness of photoresist (SU8 1075 Gersteltec). Then the wafer was aligned and exposed on a mask aligner where the mask was aligned to the markers defined by the first layer of photoresist. Finally the mold was subjected to a hard baking at 160 °C in the oven for 2 hours to improve the sidewall smoothness and the adhesion to substrate. Then the mold was treated with trimethylchlorosilane vapor (TMS, Sigma Aldrich) to prevent adhesion during PDMS casting. A 5 mm thickness of PDMS prepolymer (10 : 1 mixture of the base and curing agent, Sylgard 184, Dow Corning) was poured onto the master mold and cured in an oven for 1 hour at 100 °C. The PDMS cast was then carefully peeled off from the mold. After oxygen plasma treatment for 20 seconds, the structured PDMS was brought into contact with another flat PDMS piece to get permanent bonding. The chip was then packaged with optical fibers. Before the fiber (step index multimode fiber

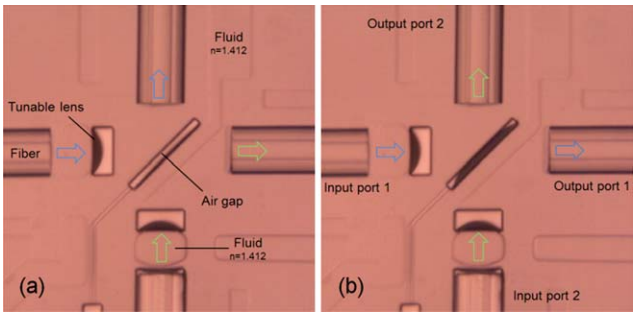

Fig. 4 Microscopy images of the device at the switching mode of exchange (a) and bypass (b).

with core diameter of 50 μm, out diameter of 125 μm, 0.22 NA, Thorlabs) was inserted into each of the four ports, the channels were filled with PDMS prepolymer through the bottom channels. This procedure was critical as the PDMS prepolymer functioned as an excellent lubricant for fiber insertion. In addition, after being cured, the filled PDMS acted as an index matching material for reducing light scattering. The fibers were fixed to the chip by UV glue. Fig. 4 shows microscopy pictures of the chip. Parts of microfluidic channels (refer to Fig. 2) were filled with index-matching liquid (refractive index 1.412) which was prepared by mixing of dimethylsulfoxide (DMSO) and water. The measured width of the air-gap is 20 μm. The micro-lenses structures have a width 125 μm and height 125 μm, in which the fluid chambers were also filled with index-matching liquid. Both the flexible membranes in the tunable air-gap mirror and lens have the thickness of 20 μm.

4. Characterization of the optofluidic switch

During characterization, a helium laser (632 nm, 15 mW) was coupled into a fiber that worked as the light source. The signal was detected by a photodiode (FDS010, Thorlabs) which directly connected to an oscilloscope (Tektronix). The air pressure was controlled by the air regulator (100-AB, Air Control Inc.) and measured by a digital pressure gauge (Omega DPG4000). The pressure switching was controlled by a miniature electromagnetic

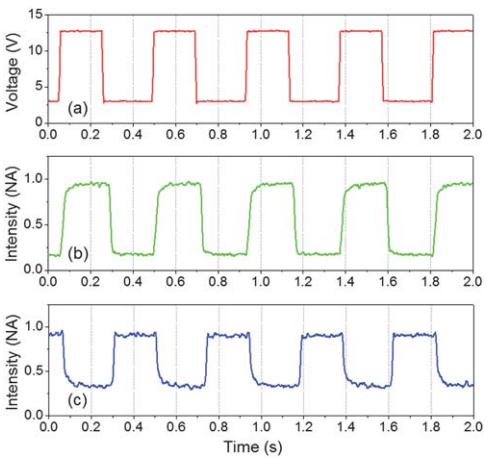

Fig. 5 The dependence of the extinction ratio with pressure applied onto the liquid lens.

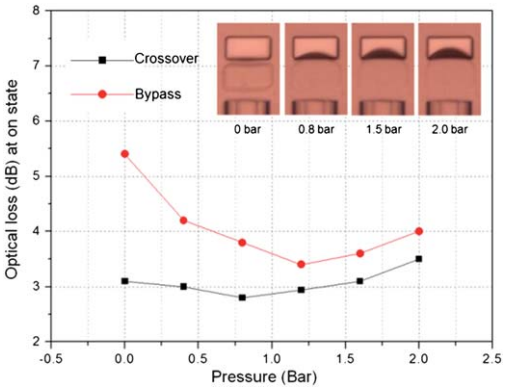

Fig. 6 The plots with square and circle shape dots represent the crossover and bypass mode respectively. The insets are the microscopy pictures of the lens at different pressures.

3-way valve (Lee Company) which was driven by a homemade amplifier circuit and an electrical function generator and homemade amplifier circuit. The tube for controlling the switch was first filled with a short section of index-matching liquid and then connected to the chip. The other end of the tube connected to the valve. The valve was able to set the pressure from ambient to a high pressure. Such pneumatical control has been widely utilized in microfluidic chips for fluid control based on the membrane valves and pumps.[38]

Fig. 4(a) and (b) show the microscopy pictures of the switch in bypass and crossover states respectively. In the bypass state, the air-gap channel was switched to the ambient pressure. In the crossover state, it was switched to the high pressure provided by the air regulator. As shown in Fig. 2(b), the light was launched into input 1, the outputs 1 and 2 were connected to the photodiodes. Fig. 5 shows the typical waveforms of different signals in a same timeline. Fig. 5(a) is the driving voltage of the electromagnetic valve. Fig. 5(b) and (c) are the normalized intensity from the output ports 1 and 2. Here we used a square wave to drive the valve with a switching frequency of about 2.3 Hz. The air pressure was switched between 0 and 1.1 bar.

The micro-lenses included in the PDMS chip are also pneumatically tunable allowing us to optimize the coupling efficiency of the fiber into the microfluidic circuit. To find the optimal focal

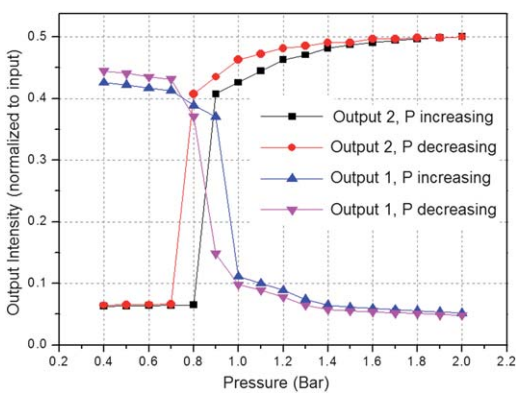

Fig. 7 The plot of the output signal from ports 1 and 2 with different pressures.

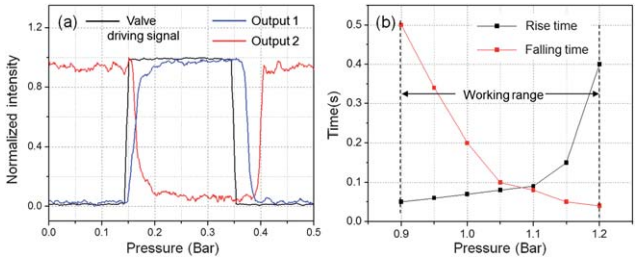

Fig. 8 (a) Wavegraph of the normalized signals of valve driving voltage and outputs of the switch. (b) The dependence of rising and falling time on the switching pressure for the signal from output port 1.

length of the micro-lens, we tuned the lens by applying different pressures and measured the optical loss at each output when the light is "on". The results are shown in Fig. 6. We found that the optimal pressure was around 1 bar to get the minimal loss. The insets in Fig. 6 are the microscopy pictures of the micro-lens at different pressures.

We also characterized the optofluidic switch in the static mode by continually adjusting the pressure applied onto the switch. Fig. 7 shows the light intensity of outputs 1 and 2 (normalized to the intensity of the input) at different pressures. In this measurement, the laser was connected to input port 1; the pressure applied to the micro-lens was fixed to 1 bar. The measurement was done twice: from low to high pressure and then from high to low pressure. The dots with triangular (square) and diamond (circle) shape represent the signal of output port 1 (port 2) when the pressure was increasing or decreasing respectively. An extinction ratio of 8 dB was achieved when the applied pressure reached 1.2 bar. We also found that the extinction ratio

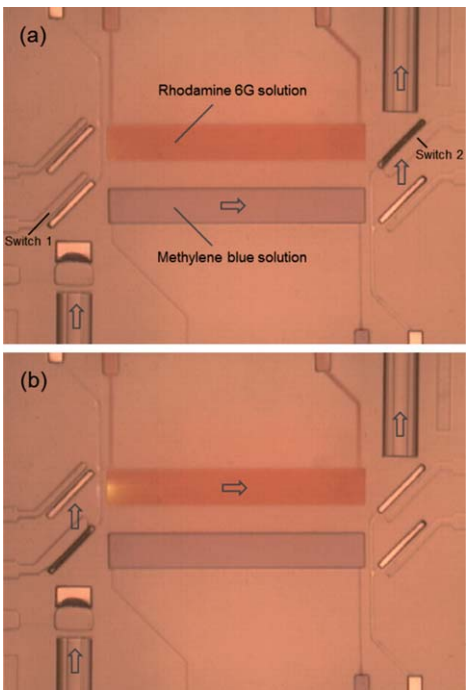

Fig. 9 Microscopy images of the chip for dual channel spectroscopy. In (a) and (b) the beam passed through the microfluidic absorption cell filled with methylene blue and Rhodamine 6G solution respectively.

Table 1 The optical extinctions at different configurations of the switches

Pressure at switch 1/bar	0	1.2	0	1.2
Pressure at switch 2/bar	0	0	1.2	1.2
Extinction ratio/dB	23.8	11.2	10.6	21.5

can be different at a given pressure. This hysteresis effect is attributed to the shape memory effect of PDMS and the adhesion when the PDMS membrane touched the other side of the air-gap channel. We repeated such measurements of the extinction ratio when input 2 was connected to the laser source; very similar results were obtained, which was inconsistent to with the symmetric design of the switch.

To further understand the dynamics of the switch, we plotted the normalized signals of the valve driving voltage *versus* the output, as shown in Fig. 8(a). The pressure was switched between 0 and 1.1 psi with a frequency of 2.3 Hz. From the graph, we can see that the signals at ports 1 and 2 complement each other. When the pressure was turned on, the switch responds rapidly as the membrane is pushed with the high pressure. When the pressure was turned off, the membrane took longer to recover, driven by the elasticity of PDMS. We measured the signal from output port 1 to characterize the dynamic response of the switch, as shown in Fig. 8(b) of the dependence of rise and fall times on the switching pressure. As the pressure increases, the rise time decreases but at the same time the fall time increases. There are two main factors accounting for the increase of the fall time. First, when the pressure was removed, the membrane of the air-gap mirror bounced back, driven by its own elastic force. As the higher pressure induces larger displacement the membrane takes longer to restore to its original state. Meanwhile the adhesion between two inner PDMS surfaces within the air-gap is also pressure-dependent. The second factor restricting the rise of the fall time was the degradation of the speed of the electromagnetic valve. The working range of the switch was found to be between 0.9 and 1.2 bar. Below 0.9 bar, the switch failed to work as the air-gap mirror took much longer to collapse. From the plot, we found the sum of rising and falling time reached the minimum of about 17 ms when the pressure was 1.08 bar. Thus the

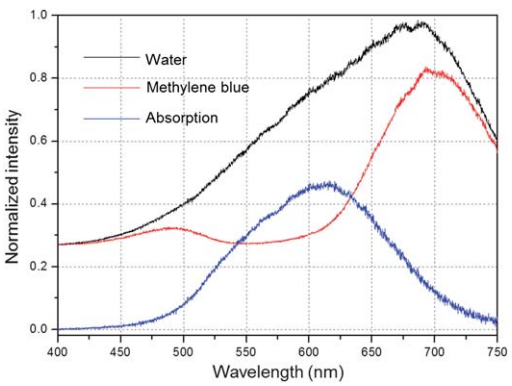

Fig. 10 The directly measured spectrum from the output fiber when the microfluidic channel was filled with water (black line) and methylene blue in water solution (red line). The plot in blue is the calculated absorption spectrum of methylene.

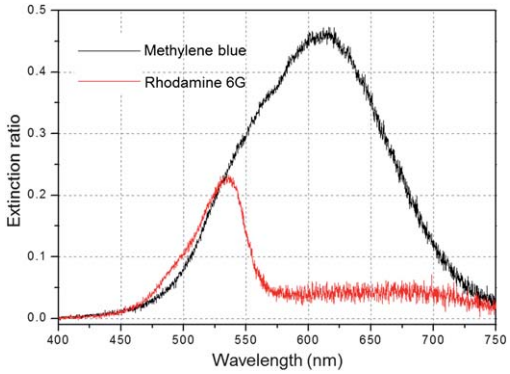

Fig. 11 The measured absorption spectrum of methylene blue (black line) and rhodamine (red line) on water solution.

maximum switching frequency of this device was estimated to be about 5.7 Hz which was in agreement to our experimental observation.

5. Dual-channel spectroscopy on a chip

As an example of the application, we demonstrated a simple reconfigurable light circuit by integrating two optofluidic switches on a single microfluidic chip. A dual-channel microfluidic absorption measurement was presented, in which the beam propagation route was selective by the switches, Fig. 9(a) and (b) show the pictures of the chip at two different configurations. The chip is mainly composed of two identical microfluidic absorption cell, a pair of air-gap mirror and a pair of optofluidic switch. By controlling the switches 1 and 2, the input beam could go through either one of the two absorption cells. In Fig. 9(a), switch 2 had high pressure (1.2 bar). So the beam passed through the bottom microfluidic channel which contained a methylene blue water solution. When switch 1 had high pressure (1.2 bar), the beam went through the top microfluidic channel which contained a Rhodamine 6G water solution.

During the experiment, the input fiber was connected to a wideband light source (Dolan-Jenner, PL-800 Illuminator); the output fiber was connected to a spectrometer (Shamrock 500 Imaging Spectrometer). Before filling the analyte, both the microfluidic absorption cells were filled with pure water to get the reference spectrums. The optical extinction at each configuration was also measured; the results are shown in Table 1. After this, the microfluidic cells were filled with the dye solutions respectively. The methylene blue solution had a concentration of 9×10^{-5} mol L^{-1}; the Rhodamine 6G solution had a concentration of 1×10^{-4} mol L^{-1}. Fig. 10 shows a normalized spectrum graph from the output fiber when the bottom cell (refer to Fig. 9) was filled with pure water (black line, reference signal) and methylene blue water solution (red line). Although the total optical loss was large in this optical circuit, by making subtraction to the reference spectrum, we got the absorption spectrum of methylene blue solution (blue line). Fig. 11 shows the measured absorption spectrum of methylene blue (black line) and rhodamine (red line) solution respectively. These results were confirmed by an additional experiment obtained using the normal cuvette.

6. Conclusion

In conclusion, we presented a pneumatically tunable 2×2 optofluidic switch which was incorporated into a PDMS based microfluidic chip. Light switching was realized with a tunable air-gap mirror that was actuated by the compressed air. The device takes the advantages of simplicity in both fabrication and operation, and it is ready to be integrated with other microfluidic structures. We also demonstrated a reconfigurable light circuit for dual-channel absorption spectroscopy measurement. We believe that the integration of such tunable optofluidic switches with state-of-the-art optofluidic components can pave the way for more complicated reconfigurable optical circuits on a chip.

References

1 D. Psaltis, S. R. Quake and C. Yang, *Nature*, 2006, **441**, 381–386.
2 C. Monat, P. Domachuk and B. J. Eggleton, *Nat. Photonics*, 2007, **1**, 106–114.
3 Z. Li, Z. Zhang, T. Emery, A. Scherer and D. Psaltis, *Opt. Express*, 2006, **14**, 696–701.
4 D. V. Vezenov, D. T. Mayers, R. S. Conroy, G. M. Whitesides, P. T. Snee, Y. Chan, D. G. Nocera and M. G. Bawendi, *J. Am. Chem. Soc.*, 2005, **127**, 8952–8953.
5 S. K. Y. Tang, Z. Li, A. R. Abate, J. J. Agresti, D. A. Weitz, D. Psaltis and G. M. Whitesides, *Lab Chip*, 2009, **9**, 2767–2771.
6 S. K. Y. Tang, R. Derda, Q. Quan, M. Loncar and G. M. Whitesides, *Opt. Express*, 2011, **19**, 2204–2215.
7 X. Mao, J. R. Waldeisen, B. K. Juluri and T. J. Huang, *Lab Chip*, 2007, **7**, 1303–1308.
8 S. K. Y. Tang, C. A. Stan and G. M. Whitesides, *Lab Chip*, 2008, **8**, 395–401.
9 D. B. Wolfe, R. S. Conroy, P. Garstecki, B. T. Mayers, M. A. Fischbach, K. E. Paul, M. Prentiss and G. M. Whitesides, *Proc. Natl. Acad. Sci. U. S. A.*, 2004, **101**, 12434–12438.
10 X. L. Mao, S. C. S. Lin, M. I. Lapsley, J. J. Shi, B. K. Juluri and T. J. Huang, *Lab Chip*, 2009, **9**, 2050.
11 A. Llobera, R. Wilke and S. Buttgenbach, *Talanta*, 2008, **75**, 473–479.
12 A. Llobera, S. Demming, R. Wilke and S. Buttgenbach, *Lab Chip*, 2007, **7**, 1560–1566.
13 S. K. Y. Tang, C. A. Stan and G. M. Whitesides, *Lab Chip*, 2008, **8**, 395–401.
14 C. Song, N. Nguyen, S. Tan and A. K. Asundi, *Lab Chip*, 2009, **9**, 1178–1184.
15 B. S. Schmidt, A. H. J. Yang, D. Erickson and M. Lipson, *Opt. Express*, 2007, **15**, 14322–14334.
16 A. H. J. Yang and D. Erickson, *Lab Chip*, 2010, **10**, 769–774.
17 S. K. Y. Tang, C. A. Stan and G. M. Whitesides, *Lab Chip*, 2008, **8**, 395–401.
18 S. K. Y. Tang, A. R. Z.LiAbate, J. J. Agresti, D. A. Weitz, D. Psaltis and G. M. Whitesides, *Lab Chip*, 2009, **9**, 2767–2771.
19 W. Song, A. E. Vasdekis, Z. Li and D. Psaltis, *Appl. Phys. Lett.*, 2009, **94**, 05117.
20 W. Song, A. E. Vasdekis, Z. Li and D. Psaltis, *Appl. Phys. Lett.*, 2009, **94**, 161110.
21 U. Levy and R. Shamai, *Microfluid. Nanofluid.*, 2008, **4**, 97–105.
22 W. Z. Song, X. M. Zhang, A. Q. Liu, C. S. Lim, P. H. Yap and H. Hosseini, *Appl. Phys. Lett.*, 2006, **89**, 203901.
23 D. Erickson, T. Rockwood, T. Emery, A. Scherer and D. Psaltis, *Opt. Lett.*, 2006, **31**, 59–61.
24 F. B. Arango, M. B. Christiansen, M. Gersborg-Hansen and A. Kristensen, *Appl. Phys. Lett.*, 2007, **91**, 223503.
25 S. Kuiper and B. H. W. Hendriks, *Appl. Phys. Lett.*, 2004, **85**, 1128.
26 J. Heikenfeld, K. Zhou, E. Kreit, B. Raj, S. Yang, B. Sun, A. Milarcik, L. Clapp and R. Schwartz, *Nat. Photonics*, 2009, **3**, 291–296.
27 H. You and A. J. Steck, *Appl. Phys. Lett.*, 2010, **97**, 023514.
28 K. S. Lee, S. B. Kim, K. H. Lee, H. J. Sung and S. S. Kim, *Appl. Phys. Lett.*, 2010, **97**, 021109.
29 H. Schmidt and A. R. Hawkins, *Microfluid. Nanofluid.*, 2008, **4**, 3–16.

30 A. H. J. Yang, S. D. Moore, B. S. Schmidt, M. Klug, M. Lipson and D. Erickson, *Nature*, 2009, **457**, 71–75.
31 A. Llobera, V. J. Cadarso, M. Darder, C. Domínguez and C. Fernández-Sánchez, *Lab Chip*, 2008, **8**, 1185–1190.
32 K. Campbell, A. Groisman, U. Levy, L. Pang, S. Mookherjea, D. Psaltis and Y. Fainman, *Appl. Phys. Lett.*, 2004, **85**, 6119.
33 Y. C. Seow, S. P. Lim and H. P. Lee, *Appl. Phys. Lett.*, 2009, **2009**(95), 114105.
34 N. T. Nguyen, T. F. Kong, J. H. Goh and C. L. Low, *J. Micromech. Microeng.*, 2007, **17**, 2169–2174.
35 W. Song and D. Psaltis, *Appl. Phys. Lett.*, 2010, **96**, 081101.
36 J. Shi, Z. Stratton, S. S. Lin, H. Huang and T. J. Huang, *Microfluid. Nanofluid.*, 2010, **9**, 313–318.
37 J. E. Fouquet, *Optical Fiber Communication Conference*, 2000, 1, 204–206.
38 M. A. Unger, H. P. Chou, T. Thorsen, A. Scherer and S. R. Quake, *Science*, 2000, **288**, 113–116.

